Hybrid incompatibility emerges at the one-cell stage in interspecies *Caenorhabditis* embryos

Jessica Bloom[1], Rebecca Green[2*], Arshad Desai[2,3], Karen Oegema[2,3*], Scott A. Rifkin[1*@]

1 Department of Ecology, Behavior, and Evolution, School of Biological Sciences, University of California, San Diego, La Jolla, CA 92093, USA

2 Department of Cell and Developmental Biology, School of Biological Sciences, University of California, San Diego, La Jolla, CA 92093, USA

3 Department of Cellular and Molecular Medicine, University of California San Diego, La Jolla, California 92093, USA.

@ Lead Contact: Scott A. Rifkin (sarifkin@ucsd.edu)

*Corresponding authors: Scott A. Rifkin (sarifkin@ucsd.edu), Rebecca Green (regreen@ucsd.edu), Karen Oegema (koegema@ucsd.edu)

SUMMARY:

Intrinsic reproductive isolation occurs when genetic divergence between populations disrupts hybrid development, preventing gene flow and reinforcing speciation.[1–4] Molecular mechanisms explaining a few dozen cases of hybrid incompatibility have been uncovered in animals,[5] including mismatches in zygotic gene regulation,[6–11] symbiont-driven incompatibilities,[12] nucleoporin mismatches affecting nuclear-cytoplasmic transport,[13] and divergence in centromeric or heterochromatic regions and their regulatory proteins that lead to the inability of the oocyte cytoplasm to segregate sperm-derived chromosomes[14–19]. Expanding mechanistic work to more diverse taxa is important for elucidating broader patterns of hybrid incompatibility.

Here, we investigate hybrid incompatibility in *Caenorhabditis Elegans* group nematodes. Within this group, most species pairs do not mate, and hybrids typically die during embryogenesis in those that do.[20–26] Although individual embryos within a cross arrest at variable timepoints,[27,28] we show that incompatibilities typically originate between fertilization and the 4-cell stage, prior to the onset of zygotic transcription.[29–32] In *Caenorhabditis*, like most animals,[33,34] sperm deliver chromatin and centrioles into the oocyte.[35–38] After oocyte meiosis, the sperm chromatin acquires a nuclear envelope, and centrioles initiate centrosome formation.[39–41] Centrosomes remain tethered to the sperm pronucleus, which positions them near the cortex to establish anterior-posterior polarity.[42,43] We identify two key processes that are destabilized in hybrids: (1) oocyte control of sperm-derived pronuclear expansion, and (2) polar body formation. When sperm pronuclear expansion is delayed, centrosomes detach, leading to defects in polarity establishment. Hybrid embryos typically experience one or more failures of early developmental events that accumulate and eventually kill them.

KEYWORDS: intrinsic reproductive isolation, hybrid incompatibility, Caenorhabditis nematodes, cell polarity, sperm pronuclear expansion, centrosome attachment, mitotic spindle, polar body extrusion

RESULTS AND DISCUSSION

Hybrid embryos resulting from fertilization of *C. brenneri* oocytes with *C. elegans* sperm exhibit polarity defects prior to zygotic genome activation

To identify incompatibilities that impair hybrid development in *Elegans* group nematodes, we capitalized on the ability of *C. brenneri* females to be fertilized by males from multiple *Elegans* group species (**Figure 1A**). To take advantage of available tools, we started with *C. brenneri* oocytes fertilized with *C. elegans* sperm. As expected, all hybrid embryos died, compared to 2% and 6% lethality, respectively, in *C. elegans* (56/2991) and in *C. brenneri* (145/2263) (**Figure 1B**). The increased lethality of *C. brenneri* embryos likely reflects ongoing inbreeding depression in lab strains, to which *C. elegans* is less susceptible.[44,45] Brood sizes were also reduced in the hybrid by day three (**Figure 1B).**

Prior work in *C. elegans* and other distantly-related *Caenorhabditis* species has shown that zygotic transcription begins at the 4-cell stage or later,[29–32] making it a useful developmental boundary. (**Figure 1C**). Defects before the 4-cell stage reflect incompatibilities between the components of oocyte and sperm, whereas later defects may arise from mismatches in zygotic gene regulation or gene products. To determine whether hybrid defects arise before the 4-cell stage or emerge after embryos initiate tissue-specific gene expression, we mated unmarked *C. brenneri* or *C. elegans* females to *C. elegans* males carrying fluorescent reporters that label nuclei in tissues derived from the three germ layers: endoderm, mesoderm, and ectoderm[46,47] (**Figure S1A**). Because the fluorescent reporters are only expressed later in development, we filmed embryos from just after fertilization through the 4-cell stage using differential interference contrast (DIC) microscopy [48] (**Figures 1D-1E**) and then used fluorescence microscopy the next day to determine the point of arrest and whether the tissue-specific markers had turned on (**Figures S1A-S1C**). Embryos from unmarked *C. brenneri* intraspecies matings were also imaged.

Embryonic development in hybrid embryos was substantially disrupted. To interpret these defects, we drew on prior work in *C. elegans*, where oocytes lack centrioles and centrosomes.[33,34] During fertilization, the sperm contributes paternal chromatin along with a pair of centrioles that mature into centrosomes and remain associated with the sperm-derived pronucleus. The sperm pronucleus holds

the centrosomes against the cell cortex, where they signal posterior identity and trigger the formation of two opposing cortical domains: the posterior contains a PAR ("Partitioning-defective") protein complex that includes PAR-2; and the anterior contains a complex that includes PAR-6 (**Figure 1D**).[42,43,49–51] The mitotic spindle aligns along this axis, dividing the embryo into a larger anterior (AB) cell and smaller posterior (P1) cell. During the second division, the AB spindle aligns vertically, and the P1 spindle aligns horizontally, producing the stereotypical 4-cell arrangement in the genus (ABa over EMS, flanked by ABp and P2 on the anterior and posterior sides; **Figures 1C** and **1D**). Proper organization at this stage is essential for cell-cell signaling and fate specification.[43]

In *C. elegans*, *par-2* knockdown prevents posterior domain formation. As a result, the spindles in both cells orient vertically, producing a 4-cell arrangement that resembles a 4-leaf clover (Both Anterior; **Figures 1D** and **S1D**).[43,49,50,52,53] Conversely, *par-6* knockdown disrupts the anterior domain, causing both spindles to orient horizontally, resulting in a linear chain of cells (Both Posterior; **Figures 1D** and **S1D**).[49,50,52] Similar defects were observed in *C. brenneri* embryos after *par-2* or *par-6* RNAi, although the *par-6* knockdown produced Both Anterior and Both Posterior outcomes in roughly equal numbers (**Figures 1D** and **S1D**; **Video S1**). Polarity was intact in 92% (12/13) of *C. brenneri* and 95% (19/20) of *C. elegans* embryos, whereas only 7% (3/44) of hybrid embryos showed normal 4-cell stage organization. Instead, 21% (9/44) showed a Both Anterior phenotype, 9% (4/44) a Both Posterior phenotype, and 64% (28/44) exhibited other aberrant arrangements, often including mispositioned P1 cells (Other; **Figure 1E**). To directly assess polarity, we used a *C. elegans* anti-PAR-2 antibody[54] that labels the posterior cortex in *C. brenneri* embryos (25/25). In hybrids, PAR-2 localization was abnormal: 3/9 embryos lacked a defined PAR-2 domain, and 5/9 had incomplete or misplaced domains (**Figure 1F**). Only one hybrid showed correct PAR-2 localization.

To determine whether polarity defects compromised progression to mid-embryogenesis and germ layer marker expression, we imaged the embryos again the following day using both DIC and fluorescence microscopy (**Figures S1A-S1C**). Germ layer reporters were expressed in 12.5% (1/8) of Both Anterior embryos, 25% (1/4) of Both Posterior embryos, and 38% (10/26) of embryos with Other 4-

cell phenotypes. In contrast, all hybrid embryos with normal 4-cell morphology (3/3) expressed germ layer reporters before arrest.

We conclude that many hybrid embryos exhibit defects consistent with compromised anterior-posterior polarity by the 4-cell stage. These defects arise prior to zygotic transcription, suggesting an incompatibility between sperm- and oocyte-derived components. Polarity defects disrupt cell fate specification and reduce the likelihood of activating tissue-specific gene expression.

Delayed sperm pronuclear expansion leads to centrosome detachment and is the likely cause of polarity defects in *C. brenneri x C. elegans* hybrid embryos

We next sought to understand how polarity defects arise in hybrid embryos. Cortical polarity is established at the one-cell stage when the sperm-derived centrioles recruit a pericentriolar material (PCM) scaffold that anchors γ-tubulin complexes for microtubule nucleation. When held against the cortex by the sperm pronucleus, the centrosomes provide a cue that establishes cortical polarity (**Figure 2A**).[42,55–57] To determine whether centrioles from *C. elegans* sperm can recruit PCM in *C. brenneri* oocytes, we used immunofluorescence to visualize microtubules (α-tubulin) and the PCM marker γ-tubulin[56,58]. Centrosomes near the sperm pronucleus recruited γ-tubulin and nucleated microtubules in all embryos—*C. elegans* (12/12), *C. brenneri* (14/14), and hybrids (12/12) (**Figures 2B** and **S2A**), indicating that *C. elegans* centrioles form functional centrosomes in *C. brenneri* oocytes. However, whereas centrosomes in intraspecies embryos remained attached to the sperm pronucleus, in hybrids, one or both centrosomes frequently detached from the sperm pronucleus (11/12 embryos; **Figures 2B** and **S2A**).

Since cortical polarity depends on centrosomes being positioned near the cortex, we tracked centrosomes in living embryos. We mated unmarked *C. brenneri* or *C. elegans* females with *C. elegans* males expressing mCherry::SAS-4 (a stably incorporated centriolar protein; **Figure 2C**).[58] We mated unmarked *C. brenneri* males to *C. brenneri* females as a control. During polarity establishment in *C. elegans* intraspecies embryos, the two mCherry::SAS-4 marked centrosomes separated as the sperm

pronucleus approached the cortex (**Figure 2D**) and remained attached to the pronucleus throughout this period (24/26 embryos; **Video S2**). Centrosome attachment is mediated by dynein anchored to the pronuclear envelope,[59–61] which pulls centrosomes towards the pronucleus by walking towards the minus ends of centrosomal microtubules (**Figure 2E**). In contrast, in most hybrids at this stage, one centrosome had detached from the sperm pronucleus (>9 μm of separation) and migrated into the cytoplasm or along the cortex (12/15 embryos; **Figure 2E**). Although typically recaptured prior to or during pronuclear meeting (**Video S2**), centrosomes were often mispositioned relative to the two pronuclei at nuclear envelope breakdown (10/15 embryos; **Figure S2B**). Nonetheless, even in hybrids, both centrioles successfully segregated to the daughter cells (**Figure S2C**).

Perturbations that reduce pronuclear size can lead to centrosome detachment followed by recapture.[48,62] This evidence supports a model in which the small initial surface area of the sperm pronucleus limits the number of microtubule interactions, leaving space for only a single centrosome to attach. The second attaches when the pronucleus grows past a size threshold.[62] At oocyte pronuclear appearance and pronuclear meeting, the cross-sectional area of the sperm pronuclei in hybrids was about half of that in *C. elegans* embryos. In hybrids, sperm pronuclei were also smaller than the corresponding oocyte pronuclei at both stages (**Figures 2F** and **2G**). We conclude that the *C. elegans* sperm-derived pronucleus fails to properly expand in the *C. brenneri* oocyte cytoplasm, leading to centrosome detachment and mispositioning which causes the observed polarity defects.

Hybrid embryos exhibit defects in polar body extrusion and spindle morphology

Centrosome position and embryonic polarization is integral to spindle orientation and morphology (**Figure 3A**). To analyze spindle orientation, we measured the angle between the centrosome-to-centrosome spindle axis and the anterior-posterior axis of the embryo (**Figure 3B**). In 95% (161/168) of control embryos, this angle was between -7.5° and 10.6°. We observed a much larger range of angles

(-66° to 51°) in hybrid embryos (**Figure 3B**), consistent with polarity defects causing large spindle oscillations during anaphase.[48,63,64]

To examine spindle morphology, we stained fixed embryos for γ-tubulin, microtubules, and DNA (**Figure 3C**). Abnormal spindle structures—frequently including bundles of kinetochore microtubules reaching out towards clusters of mispositioned chromosomes—were seen in 9/16 hybrid embryos (**Figures 2D** and **S2B**). Unexpectedly, 12/16 hybrid embryos displayed chromosomes with a meiotic-like morphology clustered near the centrosomal asters (**Figure 3C**). In 12/27 of hybrids examined for polar body formation, no polar bodies were present, suggesting that polar body extrusion failed during both meiotic divisions. Ten embryos had a single polar body, suggesting failure to extrude either the first or second polar body (**Figure 3C**). Thus, in addition to problems with pronuclear assembly and expansion, hybris of *C. brenneri* oocytes with *C. elegans* sperm frequently failed to extrude one or both polar bodies.

To visualize spindle dynamics in real time, we mated *C. elegans* expressing mCherry-tagged SAS-4 to unmarked *C. brenneri* or *C. elegans* females and dissected the worms into media containing SiR-tubulin, a vital dye that stains microtubules. In control *C. elegans* and *C. brenneri* embryos, we observed both well-formed centrosomal microtubule asters at both poles and robust kinetochore microtubule arrays aligned toward the centrally positioned chromosomes (**Figure 3D, Video S2**). In contrast, 19/22 hybrid embryos displayed abnormal spindle morphologies. Many exhibited bundled microtubule arrays—or “spindle arms”—pointing in random directions, likely because centrosomes were attempting to capture clusters of mitotic or meiotic chromosomes that were in an atypical position when nuclear envelope breakdown occurred (**Figures 3D** and **S2D; Video S2**). In 8/22 of hybrid embryos, mitotic spindle microtubules appeared to engage meiotic spindle remnants near the embryo anterior (**Figure 3D**), supporting the conclusion from our fixed cell analysis that polar body extrusion frequently fails in hybrid embryos.[65]

Similar early defects are observed in hybrids from two other *C. brenneri* and one *C. sinica* cross within the *Elegans* group

We show above that hybrids produced by fertilizing *C. brenneri* oocytes with *C. elegans* sperm exhibit delayed expansion of the sperm-derived pronucleus and frequently fail to extrude polar bodies. These embryos suffer subsequent defects in cell polarity and spindle morphology. To determine whether these early defects are common in hybrids with *C. brenneri* and whether the severity of the developmental defects increases with phylogenetic distance, we analyzed hybrid embryos from two additional crosses: *C. brenneri* females mated with either *C. sp. 48* or *C. remanei*. *C. brenneri* and *C. elegans* are estimated to have diverged ~342 million generations (~60 million years) ago.[66,67] *C. sp. 48* is a sister species of *C. brenneri*[68] and is about one-third as divergent from *C. brenneri* at the amino acid level as *C. elegans*. *C. remanei,* while it has a more recent common ancestor with *C. brenneri* than *C. elegans* (**Figure 4A**), shows ~17% greater protein divergence than *C. elegans*. Crosses between *C. brenneri* females and *C. sp. 48* males had brood sizes comparable to intraspecies crosses, but all 2761 embryos died during embryogenesis (**Figure S3A**). Crosses between *C. brenneri* females and *C. remanei* males resulted in reduced brood sizes and nearly complete embryonic lethality (885/887 embryos died; **Figure S3A**).

To characterize early developmental defects, we scored DIC movies of intraspecies embryos as well as hybrid embryos resulting from fertilization of *C. brenneri* oocytes with sperm from the three other species for the presence of 20 early embryonic defects (~120 total movies; **Figures 4C, S3A,** and **S3B; Data S1A**). A similar spectrum of defects was observed for hybrid embryos from the three crosses, including small and/or misshapen sperm pronuclei, detached or mispositioned centrosomes, and polar body extrusion defects. We also observed signs of disrupted cell polarity, such as equally sized AB and P1 cells at the 2-cell stage and abnormal 4-cell stage arrangements (**Video S3**). *C. brenneri* x *C. sp. 48* hybrids often overcame their initial defects to reach a superficially normal 4-cell stage (**Figure 4B**). Defects in the more distant *C. remanei* and *C. elegans* crosses were more frequent and severe compared to the sister species cross, suggesting that the severity of the disruption of early developmental processes increases with evolutionary distance between the parental species.

To determine whether such early defects are specific to hybrids with *C. brenneri* mothers or occur more broadly across the *Elegans* group, we also analyzed *C. sinica* embryos and hybrids generated by

fertilizing *C. sinica* oocytes with *C. remanei* sperm (**Figures 4D-F**, **S3C,** and **S3D)**. Interestingly, while sperm pronuclei expanded slowly in hybrids generated by fertilizing *C. brenneri* oocytes with interspecies sperm (including *C. remanei*), *C. remanei* sperm pronuclei expanded prematurely after fertilizing *C. sinica* oocytes, reaching larger sizes than the sperm-derived pronuclei in either intraspecies cross (**Figures 4D, 4E** and **S3C**), showing that sperm-derived pronuclear expansion can be either too slow or too fast in hybrids. Defects in centrosome positioning and spindle orientation were also observed in the *C. sinica x C. remanei* hybrids, consistent with the mismatch in sperm and oocyte pronuclear size (**Figure S3D**). Moreover, in contrast to the normal pattern in which the larger anterior AB cell divides before the smaller posterior P1 cell— the posterior P1 cell divided first or simultaneously with the AB cell in ~25% of *sinica/remanei* hybrid embryos (**Figure 4F**). Thus, hybrids with *C. brenneri* or *C. sinica* mothers experience very early embryonic defects that eventually cascade into developmental failure.

Conclusion

Our findings suggest that incompatibility between interacting components from oocytes and sperm is a common mechanism underlying hybrid incompatibility among *Caenorhabditis Elegans* group nematodes (**Figure 4G)**. Two key drivers of incompatibility are: (1) the ability of oocytes to properly control the timing of sperm-derived pronuclear expansion and (2) the ability of fertilization to facilitate polar body formation. Electron microscopy has shown that sperm chromatin, along with the centrioles, is nested within an electron-dense, RNA-containing halo[35,37,38,69] instead of being encapsulated by a nuclear envelope. In *C. elegans*, the sperm chromatin and centrioles initially remain quiescent while the oocyte chromosomes complete their meiotic segregation. The centrioles are activated to become centrosomes, and the sperm chromatin becomes encased in a nuclear envelope and initiates pronuclear expansion.[39,40] Although the processes that remove the RNA halo and assemble an import-competent nuclear envelope around the sperm chromatin are not well understood, our data suggest that this transition is sensitive to genetic divergence and is a common locus of interspecies incompatibility. The defect may be in releasing the sperm chromatin from the RNA-containing halo or in the subsequent assembly of a transport-

competent nuclear envelope around the sperm chromatin. Our finding that divergence can disrupt the ability of oocytes to properly handle the packaged sperm chromatin has some similarity to prior work in other animal clades showing that divergence in centromeric or heterochromatic regions and their regulatory proteins can lead to an inability of the oocyte cytoplasm to segregate sperm-derived chromosomes.[14–19] More work on the molecular specifics of the sperm pronuclear expansion defects will be needed to determine how similar the mechanisms driving these incompatibilities might be. We also observed frequent failures in polar body extrusion in hybrids. The cause of the polar body extrusion failure, and whether it is related to the sperm pronuclear expansion defect, is unclear. However, SPE-11—a sperm-provided protein that localizes to the RNA-containing sperm halo—is essential for polar body formation in *C. elegans*,[65,70,71] suggesting that incompatible sperm factors could contribute to this defect.

To identify candidate proteins whose divergence may contribute to hybrid incompatibility, we extracted lists of genes in classes related to the phenotypes observed in hybrid embryos from Phenobank, a database that includes phenotypic data for *C. elegans* genes required for the first two embryonic divisions. We measured protein sequence divergence of these genes between *C. brenneri* and the other species in this study (**Figure S4**). Low divergence proteins clustered with conserved proteins like the ubiquitin gene UBQ-1,[72] and high divergence proteins clustered with sperm proteins like SPE-9 and SPE-11. Several proteins involved in the formation and structure of nuclear pore complexes, including MEL-28, NPP-7, NPP-4, NPP-23, and NPP-11,[73–79] clustered with proteins exhibiting high divergence, raising the possibility that evolution at the amino acid level could have altered the association of one or more of these components with sperm chromatin in hybrid embryos and changed the timing of sperm pronuclear expansion.

Although hybrid embryos experience problems immediately after fertilization, they do not die until later in development. The varied arrest points observed within each cross suggest that each defect incrementally destabilizes development, making subsequent events more prone to failure. While normal embryos can often recover from moderate disruptions,[80] hybrids lack such resilience. A few hybrid

247 embryos may find a narrow pathway to hatching, but most succumb to a cascading series of stochastic
248 failures that accumulate over time and produce a spectrum of fatal outcomes (**Figure 4G**).
249
250
251

RESOURCE AVAILABILITY

Lead contact

Further information and requests for resources and reagents should be directed to and will be fulfilled by the lead contact, Scott Rifkin ([31,32]).

Materials availability

All strains and other reagents generated in this study are freely available from the lead contact upon request. *C. brenneri, C. remanei, C. sinica,* and *C. elegans* (*fog-2*) strains can be obtained from the Caenorhabditis Genetics Center (CGC). *C. sp. 48* was a gift from M.-A. Félix.

Data and Code Availability

- Data reported in this paper will be available from the Lead Contact upon request.
- The custom computer code generated for this project is publicly available through https://gitlab.com/evodevosyslabpubs/Bloom_etal_2025 and Zenodo (DOI: 10.5281/zenodo.15603738).
- Any additional information required to reanalyze the data reported in this paper will be available from the Lead Contact upon request.

ACKNOWLEDGEMENTS

We would like to thank members of the Rifkin, Oegema, and Desai labs for helpful discussions. We would like to thank Anthony Hyman for the generous gift of the PAR-2 antibody and Marie-Anne Félix for the generous gift of strain BRC20359 (*C. sp. 48*). We would also like to thank Anthony Ye and Aidan Linkins for their help. This work was supported by grants from the NIH (GM103782) and the NSF IOS (1936674) to S.A.R. and from the NIH to K.O. (GM147265). K.O. acknowledges salary support from the Ludwig Institute for Cancer Research. JB was partially supported by NIH/NIGMS (T32 GM127235). Some strains were provided by the CGC, which is funded by NIH Office of Research Infrastructure Programs (P40 OD010440).

AUTHOR CONTRIBUTIONS

Conceptualization: J.B., R.G., K.O., S.A.R.; Methodology: J.B., R.G., K.O., S.A.R.; Formal analysis: J.B., R.G.; Investigation: J.B., R.G.; Resources: S.A.R., K.O.; Data curation: J.B., R.G.; Writing - original draft: J.B., R.G., K.O., S.A.R.; Writing - review & editing: J.B., R.G., A.D., K.O., S.A.R.; Visualization: J.B., R.G.; Supervision: R.G., S.A.R., K.O.; Project administration: S.A.R., K.O.; Funding acquisition: S.A.R., K.O.

DECLARATION OF INTERESTS

The authors declare no competing interests.

MAIN TEXT FIGURE LEGENDS

Figure 1. **Hybrid embryos resulting from fertilization of *C. brenneri* oocytes with *C. elegans* sperm exhibit polarity defects prior to zygotic genome activation.** (**A**) Phylogeny of the *Elegans* group of *Caenorhabditis*.[68] *C. brenneri* females have been shown to be cross-fertile with *C. elegans* (*red*) males and males from the species marked in dark grey. (**B**) Schematic illustrating how embryos were collected after mating. Graphs show the average brood size and % hatching for the embryos collected during each day of egg laying. Brood sizes were reduced in the interspecies matings, especially by day three post-mating. Day 1 is 0-24 hours post-mating; day 2 is 24-44 hours post-mating; day 3 is 44-64 hours post-mating. n refers to the number of embryos counted per cross. Error bars are ± 1 SE. **(C)** Schematic of the events between fertilization and the 4-cell stage when Zygotic Genome Activation begins. The sperm brings the sperm chromatin, which is not encased in a nuclear envelope but is instead embedded in an RNA-containing layer with a pair of centrioles,[69] into the oocyte. Once in the oocyte, a nuclear envelope assembles around the sperm chromatin to form the sperm-derived pronucleus and the centrioles form centrosomes. The larger, anterior AB cells divides first followed by the smaller, posterior P1 cell, leading to the canonical arrangement of cells at the 4-cell stage. ZGA begins, when the sperm genome is first expressed. Hybrid incompatibilities prior to this stage are due to incompatibilities between the components derived from the sperm and oocyte. (**D**) Differential interference contrast (DIC) images of 4-cell stage embryos for: (*left*) control intraspecies *C. brenneri* and *C. elegans* embryos; (*middle*) *par-2(RNAi)* and *par-6(RNAi) C. elegans* embryos; and (*right*) and *par-2(RNAi)* and *par-6(RNAi) C. brenneri* embryos. For phenotypic quantification see *Figure S1D*. The schematic on top illustrates the anterior PAR-6 (*yellow*) and posterior PAR-2 (*orange*) domains at the 1-cell stage in *C. elegans*. Schematics above the images show the expected cell and spindle orientations for two-cell and four-cell stage embryos for each condition. (**E**) DIC images illustrating the three non-wild-type classes of 4-cell stage phenotypes observed for hybrid embryos resulting from mating *C. brenneri* females with *C. elegans* males (Both Anterior, Both Posterior, and Disorganized/Other). Schematics above the images illustrate the cell and spindle orientations at the two-cell and four-cell stages for each embryo. The graph quantifies the percentage of embryos exhibiting each phenotype. (**F**) (*top*) Schematic illustrating the localization of PAR-2 and DNA in a control embryo. (*left*) Representative immunofluorescence images of *C. brenneri* (top; n = 25) and hybrid embryos (bottom; n = 9) stained for PAR-2 (*magenta*) and DNA (*cyan*). (*right*) Grayscale PAR-2 images with yellow arrowheads marking the PAR-2 domains. Scale bars, 5μm**.** See also **Figure S1** and **Video S1**.

Figure 2. Sperm pronuclear expansion is delayed in hybrid embryos, leading to centrosome detachment, which can cause polarity defects. (**A**) Schematic illustrates how fertilization triggers polarity establishment in the 1-cell embryo. The sperm brings in a pair of centrioles (*green*) that are converted to centrosomes via recruitment of a microtubule-nucleating scaffold (*red*) from the oocyte cytoplasm. The sperm pronucleus holds the centrosomes next to the cortex, where they provide a cue that specifies the embryo posterior. (**B**) (*top*) Schematic illustrates the mating regime and markers shown in the immunofluorescence images below. (*bottom*) Representative images of 1-cell stage *C. brenneri* (n = 14) and hybrid (n = 12) embryos after the conversion of centrioles to centrosomes, but prior to pronuclear migration, stained for DNA (cyan) and γ-tubulin (red). Insets are magnified 1.7X. γ-tubulin (red) is scaled equivalently in the two images. (**C**) Schematic illustrates the mating of *C. brenneri* or *C. elegans* females with *C. brenneri* males or with *C. elegans* males whose centrioles are stably marked with mCherry::SAS-4 (*green*) to allow monitoring of sperm centriole position throughout the first cell division. (**D**) Paired DIC/fluorescence overlay (*left*) and fluorescence-only (*right*) images of *C. brenneri*, *C. elegans,* and hybrid pronuclear appearance stage 1-cell embryos. The schematic on top illustrates the expected position of the mCherry::SAS-4 marked centrioles between the sperm pronucleus and cortex (*green*). The white solid lines trace the embryo. The white dashed lines trace pronuclei in DIC and fluorescence images. Insets are magnified 2.3X, and yellow arrowheads mark centrosomes. Image intensities for centrioles are scaled to highlight centriole position and cannot be compared across images. (**E**) Schematics depict wild-type-like centrosome-pronuclear attachment mediated by the interaction of centrosomal microtubules with dynein anchored to the nuclear envelope by the LINC complex[59–61] (*grey box*) and aberrant detachment (*blue box*) of centrosomes from the sperm pronucleus. Graph quantifies the percentage of embryos with centriole detachment (>9 μm separation) from the sperm pronucleus. (**F**) Graph plots the cross-sectional area of sperm pronuclei at the pronuclear appearance stage. The median (IQR) sperm pronuclear cross-sectional areas are 49 (39-58), 32 (28-37), and 16 (9-23) μm^2 for *C. brenneri*, *C. elegans*, and hybrid embryos, respectively. Centriole detachment is indicated by blue circles, and wild-type-like centriole separation is indicated by dark gray circles. (**G**) DIC images of representative *C. brenneri*, *C. elegans*, and *hybrid* embryos at pronuclear meeting. Insets are magnified 2X (the cyan and magenta dotted lines outline the sperm and oocyte-derived pronuclei, respectively). The left graph plots the cross-sectional areas of oocyte and sperm pronuclei at pronuclear meeting for the indicated crosses. Centriole detachment is indicated by blue circles and wild-type-like centriole separation by dark gray circles. In *C. brenneri*, centrioles were not labeled, and detachment was not scored (*light gray circles*). Median (IQR) of female pronuclear cross-sectional areas are 61 (51-71), 36 (30-42), 46 (26-66) μm^2 for *C. brenneri, C. elegans*, and hybrid embryos, respectively. Median (IQR) of male pronuclear cross-sectional areas are 67 (56-78), 38 (32-44), 17 (7-27) μm^2 for *C. brenneri, C. elegans*, and hybrid embryos, respectively. Right graph plots the ratio of sperm to oocyte pronuclear area at pronuclear meeting. Median (IQR) ratios for sperm pronuclear area to oocyte pronuclear areas are 1.2 (0.9-1.5), 1.1 (0.9-1.3), 0.4 (0.01-0.73) for *C. brenneri*, *C. elegans*, and hybrid embryos, respectively. n refers to the number of embryos quantified. Scale bars, 5μm. See also **Figure S2** and **Video S2**.

Figure 3. *Caenorhabditis* hybrid embryos exhibit defects in polar body extrusion and spindle morphology. (**A**) A schematic illustrating how detachment of centrosomes from the sperm pronucleus could contribute to defects in spindle positioning and spindle morphology in the early embryo. (**B**) Schematics (*top*) and images (*bottom*) illustrating how spindle orientation was assessed. At each timepoint, the angle between the centrosome-to-centrosome axis of the spindle (red dashed line) and the anterior-posterior axis of the embryo (red solid line) was measured. For each embryo, six measurements were made at 30-45 second intervals starting at metaphase. The graph plots the six measured angles for each embryo in a column. Angles were measured in *C. brenneri* (*black*), *C. elegans* (gray) or hybrid (*purple*) embryos. (**C**) Representative immunofluorescence images of *C. brenneri* (n = 8) and hybrid (n = 16) embryos are shown to illustrate hybrid phenotypes, which include abnormally structured spindles that have captured meiotic chromosomes due to failed polar body extrusion. Schematics illustrate a control mitotic spindle (top) and a mitotic spindle with an extra 'spindle arm' due to capture of meiotic chromosomes (bottom). Embryos were stained for DNA (*cyan*), microtubules (DM1-α) (*green*) and γ-tubulin (*red*). Graph on the right quantifies the distribution of the number of polar bodies in mitotic hybrid embryos. Pink arrows point to extra spindle arms. (**D**) As illustrated in *Figure 2C*, *C. brenneri* or *C. elegans* females were mated with *C. elegans* males with mCherry::SAS-4-marked centrioles to enable live tracking of centrioles (*green*). As a control, *C. brenneri* females were also mated with *C. brenneri* males. As shown in the schematic (*top*), embryos were dissected into the vital dye SiR-tubulin (*red*) to monitor microtubules. (*left*) Images are maximum intensity projections of representative intraspecies *C. brenneri* and *C. elegans* embryos and hybrids. Times are seconds relative to metaphase. Arrows indicate centrioles that separated with normal timing (white) or prematurely (yellow). Cyan arrows indicate abnormal spindle morphology. Dark blue arrows indicate meiotic spindle remnants. Insets show 2X magnifications of one anaphase spindle pole. Maximum intensity projections were made of all z-planes containing the centrosomes and spindle structures, and SiR-tubulin intensities were scaled to best show spindle morphology and cannot be directly compared. (*right*) Graphs quantify the percentage of embryos exhibiting premature centriole separation (*yellow*), and abnormal spindle morphology (*cyan*) for the indicated conditions. Scale bar, 5μm. See also **Figure S2** and **Video S2**.

Figure 4. **Similar phenotypic defects are observed in hybrid embryos generated by fertilization of *C. brenneri* oocytes with sperm from three Elegans group species. (A)** (*Left*) Phylogeny of the *Elegans* group. In the experiments in *B* and *C*, *C. brenneri* (*black*) females were mated with males from three species: *C. remanei, C. sp. 48,* and *C. elegans (indicated in red). For D-F, C. sinica* (black) females were mated with *C. remanei* males. (**B**) DIC images from timelapse series of representative embryos showing them at the 1, 2, and 4-cell stages for all intraspecies (*red and black labels*) and interspecies crosses (*purple labels*). Solid white lines trace the outline of each cell; dotted cyan and magenta lines trace the sperm and oocyte-derived pronuclei, respectively. (**C**) The heatmap summarizes embryonic defects observed through the 4-cell stage for the indicated crosses; embryos were scored blinded to cross. Shading from white to dark blue indicates phenotype penetrance. Centrosome positioning defects are likely under-counted (compared to *Figure 2D*,*E*) because it is difficult to accurately follow centrosomes without a fluorescent marker. Aspect ratio scored as defective if it was outside of 2 standard deviations of the average across all wild-type embryos. (**D**) DIC images from timelapse series of representative embryos showing them at the 1, 2, and 4-cell stages for intraspecies *C. sinica* embryos (*C. remanei* shown in *B*) and the interspecies cross of *C. sinica* females to *C. remanei* males to (*purple labels*). Solid white lines trace the outline of each cell, dotted cyan and magenta lines trace the sperm and oocyte-derived pronuclei, respectively. The *C. remanei* sperm-derived pronucleus expands prematurely after it enters the *C. sinica* oocyte (see also *Figure S3C*). (**E**) The graph quantifies the cross-sectional area of sperm pronuclei at the pronuclear appearance stage. Median (IQR) for sperm pronuclear cross-sectional areas are 46 (37-55), 47 (42-52), and 57 (43-71) μm^2 for *C. sinica, C. remanei*, and hybrid embryos, respectively. (**F**) (*left*) After polarity establishment, the anterior AB cell divides prior to the posterior P1 cell, as observed in the dividing 2-cell intraspecies *C. remanei* and *C. sinica* embryos shown. In contrast, in the hybrid embryo shown, the P1 cell is undergoing cytokinesis before the AB cell. (*right*) The graph quantifies the AB/P1 division order in the embryos filmed for each condition. (**G**) A schematic illustrating the cascade of stochastic developmental failures in hybrid embryos. In hybrid embryos, a number of early embryonic events become more prone to failure, including polar body extrusion and the formation and expansion of the sperm pronucleus. These defects can, in turn, lead to centrosome detachment and defects in polarity establishment or 2-cell stage division timing. If hybrid embryos successfully navigate these early events, additional defects arise after the zygotic genome is activated and cell fate specification begins. Hybrid embryos exhibit a broad range of arrest points, and few survive to hatching. Scale bars, 5μm. See also **Figure S3, Figure S4, Data S1,** and **Video S3**.

STAR METHODS

EXPERIMENTAL MODEL AND STUDY PARTICIPANT DETAILS

C. elegans, C. brenneri, C. sp. 48, C. sinica, and *C. remanei* strains were maintained at 20°C on standard Nematode Growth Media (NGM) plates seeded with OP50 bacteria. The genotypes of the *C. elegans* strains used in this study are described in Reagents and Resources.

METHOD DETAILS

Strains

The following strains were used for experiments (see key resources table for details): *C. brenneri* wild-type LKC28; *C. sp. 48* wild-type BRC20359; *C. remanei* wild-type EM464; *C. sinica* wild-type JU1201; and *C. elegans* JK574 females and males, which has a *fog-2* mutation that makes hermaphrodites females and produces an increased number of males compared to *C. elegans* N2.

Mating

For all crosses, L4-stage females were placed with males on a 35mm plate seeded with OP50 and left overnight at 20C for mating; females were dissected the following day. A 1:2 ratio of females to males was used for all crosses except for interspecies crosses with *C. elegans* males, for which a 1:3 ratio was used because C*. elegans* males are worse at mating than dioecious males.[84,85]

Dissections

Gravid females were dissected in Boyd Buffer (59.9 mM $NaCl_2$, 32.2 mM KCl, 2.8 mM Na_2HPO4, 1.8 mM $CaCl_2$, 5mM HEPES pH 7.2, 0.2% glucose, 2.1 mM $MgCl_2$;)[53,86] and were transferred by mouth pipette to a 2% agarose pad made in Boyd Buffer for imaging. An 18x18mm coverslip was placed over the pad and the edges of the coverslip were sealed with VALAP (1:1:1 Vaseline, Lanolin, and Parafin) to prevent drying out. We compared five different osmotic support buffers (meiosis media, Boyd buffer, 0.5X Egg Salts, 0.7X Egg Salts, and 1X Egg Salts)[53,86–88] but no rescue of early arrest phenotypes was observed for any of them.

Brood size & embryonic viability measurements

To measure the number of embryos laid and assess their viability (defined hatching), individual L4 females were placed on a 35 mm NGM plate seeded with OP50 along with 2 or 3 males (see Mating section) and left to mate overnight at 20°C. After 24 hours, the males were removed and the females were moved to a second 35mm plate. Females were transferred again to a third 35 mm plate 20 hours later (44 hours after the start of mating). After 64 hours, the females were removed from the third plate. After each transfer, the number of freshly laid embryos on the plate from which the female was removed

was counted and the plate was returned to 20°C. Since viable embryos hatch within 20 hours of being laid we waited 20-24 hours after first count was made and then counted the number of hatched and unhatched embryos to measure viability.

RNA production

The *C. brenneri* orthologs of the *C. elegans par-2* and *par-6* genes were identified based on annotation in WormBase; ortholog identity was confirmed using reciprocal BLAST. DNA templates for generating dsRNAs were generated by PCR using primers designed using Primer3 (https://primer3.ut.ee/) to amplify a 400-800 bp region of each gene from genomic DNA (see KEY RESOURES Table for sequences). Primers contained T3 or T7 promoters to enable transcription reactions. Primers for dsRNAs targeting the *C. elegans* genes were the same as those employed in a prior RNAi-based screen.[48] PCR reactions were cleaned and used as templates in T3 and T7 transcription reactions. T3 and T7 RNA products were mixed at equimolar amounts, cleaned, and annealed by adding 3X Soaking buffer (32.7 mM Na_2HPO_4, 16.5 mM KH_2PO_4, 6.3 mM NaCl, 14.1 mM NH_4Cl) to a final concentration of 1X and incubating reactions at 68C for 10 minutes then 37°C for 30 minutes.

RNA interference

For *C. elegans*, larval (L4 stage) female (JK574) worms were injected with dsRNA in the body cavity and left to recover at 20°C for 4 hours before singling and mating with male *C. elegans* (JK574) worms at 20°C and left overnight before imaging. For *C. brenneri*, larval (L4 stage) females (LKC28) were mated to male *C. brenneri* (LKC28) worms on a 35mm OP50 plate overnight at 20°C. Gravid females were injected with dsRNA in both gonad arms, left to recover for 3 hours (20°C), before singling and leaving overnight at 20°C for 22 hours before imaging.

Imaging and analysis of early and late embryogenesis

After mating, dissection, and mounting as described above, we monitored early embryogenesis using differential interference contrast (DIC) optics to acquire 26 x 1µm z-stacks at 30-45 second intervals. In most experiments, embryos were imaged through the four-cell stage. Images were acquired using either an inverted Zeiss Axio Observer Z1 system equipped with a Yokogawa CSU-X1 spinning-disk, 63X 1.40 NA Plan Apochromat lens (Zeiss), and a QuantEm: 512SC camera (Teledyne Photometrics), or on a Nikon Ti2 microscope equipped with a Yokogawa CSU-X1 spinning disk, a 60X, 1.4 NA PlanApochromat lens, and an iXon Life EMCCD camera. For monitoring fluorescent marker turn-on, embryos that had been filmed by DIC during early embryogenesis were allowed to develop for 20 additional hours at 20°C before the acquisition of 26 x 1µm z-stack using confocal fluorescence microscopy (488 and 561 nm lasers) and DIC optics. For all measurements, embryos were cropped from time-lapse series and measurements were made using FIJI.[89] **Data S1B** has descriptions of the features scored or measured.

Centriole Positioning in Early Hybrid Embryos

C. elegans (OD3701) or *C. brenneri* (LKC28) males were crossed to *C. brenneri* (LKC28) or *C. elegans* (JK574) females and left to mate overnight at 20°C for 24 hours. Female worms were dissected and embryos mounted as described above. Embryos were imaged by collecting 19 x 1.5 µm z-stacks every 30 sec, capturing DIC and fluorescence (561nm laser at 15% power, 2x2 binning, 100ms exposure) through the two-cell stage. FIJI was used to crop and rotate images for scoring. Centrioles were

considered detached when centrioles were > 9µm apart. FIJI was used to create maximum projections and to scale images for figures. The image intensities were scaled to best visualize centrosome position within the early embryo.

Spindle Angle, Pronuclear Localization and Size, and Embryo Aspect Ratio Analysis

Embryos were cropped from timelapse series and measurements were made using FIJI. P0 spindle angle was measured relative to the long axis of the embryo; the angle was assessed from metaphase onset through the following 3.5-4.5 minutes. Images were converted to maximum intensity projections, since centrioles were in different z-planes for part of the first cell division, and then each embryo was scored for centrosome detachment before pronuclear meeting or centrosome mis-localization at pronuclear meeting. Sperm pronucleus length and width was measured at the appearance of the oocyte-derived pronucleus, and sperm-derived pronuclear area was then calculated by using the equation for the area of an ellipse : $\pi \frac{leng}{2} \frac{widt}{2}$. Embryo aspect ratio was calculated as the ratio of cross-sectional width to cross-sectional length of P0 embryos.

Centriole Positioning and Microtubule tracking

C. brenneri (LKC28) females were crossed with *C. brenneri* (LKC28) males or *C. elegans* (OD3701) males, and *C. elegans* (JK574) females were crossed with *C. elegans* (OD3701) males. Female worms were dissected into 250 nM SiR-tubulin dye (Cytoskeleton, cat# CY-SC002). To generate an agar pad containing SiR-tubulin, 15µL of 5µM dye was added on top of a 2% agarose pad made in Boyd Buffer. One-cell embryos were transferred by mouth pipette, covered with an 22x22mm coverslip, and sealed with VALAP before imaging. Embryos were imaged on a Nikon Ti2 microscope equipped with a Yokogawa CSU-X1 (Nikon) spinning disk, a 60X, 1.4 NA PlanApochromat lens, and an iXon Life EMCCD camera. A 27 x 1 µm z-stack was collected every min, capturing DIC and fluorescence (561nm at 15% power, 2x2 binning, 100ms exposure, and 640nm at 40% power and 200ms exposure) through the two-cell stage. Images were cropped and rotated for analysis using FIJI. Timelapse SiR-tubulin sequences were created by generating maximum intensity projections of the best subset of 14 z-slices containing the spindle and were scaled to show the best signal unobscured by the SiR-tubulin coating the eggshell. Image intensities were scaled independently for each embryo because dye uptake varies between embryos. Centriole channel images were created using maximum projections to best capture the centrioles.

Developmental Imaging

For the arrest point experiment in **Figures S1A** and **S1C**. *elegans* males (OD 1719)[46] or *C. brenneri* males (LKC28) were mated with *C. elegans* females (JK574) or *C. brenneri* females (LKC28) for 24hrs at 20°C. OD1719 animals express germ-layer markers: ectoderm (Pdlg-1::mCherry::his-72 and Pcnd-1::mCherry::his-72), endoderm (Ppha-4::pha-4::GFP), and mesoderm (Phlh-1::his-72::mCherry and Phlh-1::his-72::GFP). For this experiment, embryogenesis was captured by dissecting females in Boyd Buffer and transferring the embryos to a 384-well imaging plate containing 70uL Boyd Buffer. Embryos were imaged over a 10-hour time-course as previously described.[46]

Immunofluorescence of Early Embryos

Slides for immunofluorescence were generated by dipping in subbing solution prepared by dissolving 0.1g gelatin in 25 mL of distilled water heated to 60°C, cooling to 40°C, adding 0.01g chromalum, and 15mg poly-lysine HBr. Subbing solution was left to stir at 40°C for 2 hours before sterile filtering and storage at 4°C. Slides were dipped in subbing solution heated to 50°C and allowed to dry for 6 hours. 20-30 mated female animals were placed in a 4µl drop of distilled water placed in the center of the slide and an 18x18 coverslip was placed on top. Worms were compressed by pushing on the coverslip with a pipet tip, embryos were pushed out of the mothers, and slides were plunged into liquid nitrogen. Slides were retrieved and a razor blade was used to pop the coverslips off each slide. Slides were immediately immersed in -20°C cold methanol for a 15-minute fixation. Samples were fixed and stained as previously described.[90] For detection of PAR-2, slides were incubated in unconjugated primary antibody (Mouse-anti-PAR-2 1:1000 dilution) overnight at 4°C, washed, and then incubated with fluorescent secondary antibody (Donkey-anti-Mouse-Cy5) for 30min at room temperature. To stain for centrosomes and microtubules, embryos were incubated with directly-labeled α-tubulin antibodies (DM1-α-FITC 1:1000 dilution; Sigma Aldrich F2168) and anti-γ-tubulin-CY3 (C-terminal antigen: LDEYKAVVQKDYLTRGL; 1:300 dilution)[55] for 60 minutes at room temperature. Slides were washed with PBST buffer, and 1 µg/ml Hoechst was added during the last 10-minute wash. Two final washes were performed and 15 µl of ProLong Glass Antifade Mount (ThermoFisher) mounting and curing solution was added before covering the embryos with an 18 x 18mm coverslip. The slides were left to cure at room temperature for 24 hours in a dark chamber. Samples were imaged on a DeltaVision (GE Healthcare) epifluorescence scope equipped with a 100X 1.4NA oil immersion objective. Images were deconvolved using SoftWoRx software (Cytvia). Maximum projections were made using FIJI and image intensities adjusted for best visualization of signal.

Analysis of hybrid embryos

C. brenneri females were mated to males of *C. sp. 48*, *C. remanei*, and *C. elegans* as described above. *C. sinica* females were mated to *C. remanei* males as described above. Embryos were dissected and DIC images of early embryogenesis were acquired as described above collecting images every 30s until the 4-cell stage or later. Embryos were cropped and rotated for further analysis. Image names were anonymized by JB, and embryos scored by RG as either a 1 (display phenotype) or 0 (do not display phenotype) for the phenotypes listed in **Data S1B**.

Divergence time estimates

We downloaded complete *Caenorhabditis* genomes from download.caenorhabditis.org,[89] extracted the longest isoforms for each protein, and used the species tree estimated by Orthofinder. Branch lengths of the estimated species tree represent molecular phylogenetic distance along the branch.[91] We used these branch lengths to determine the relative divergence of protein coding sequences between *C. brenneri* and the three other species.

Sequence Analysis

Protein sequences for analysis were chosen based on membership to the following phenotype categories on Phenobank when targeted by RNA interference: Pronuclear/Nuclear appearance, Centrosome attachment, Asymmetry of Division. In addition, proteins known to be highly conserved such as BEN-1, and proteins of high divergence, such as sperm proteins (SPE-9, SPE-11) were included as points of comparison for divergence scores. The *C. elegans* ortholog for each gene of interest was then used to

collect all possible orthologs for *C. brenneri, C. remanei, C. sp. 48*, and *C. sinica* using Orthofinder (Emms 2019) using the default settings. Each ortholog from all species was then locally aligned to the *C. elegans* ortholog from Phenobank using a BLOSUM62 scoring matrix. Orthologs with the highest scores were then used for global pairwise sequence alignment. Alignment scores for each protein were collected in a 2D distance matrix. Distance matrices were then converted to 1D and used to generate heat maps. Only proteins with an identified ortholog for every species analyzed were included in the larger heat map of *C. brenneri* divergence scores. Hierarchical clustering of *C. brenneri* specific divergence scores was generated using R (Rstudio)[92] (hclust(), method = "complete") and protein name labels were generated using SimpleMine (https://wormbase.org//tools/mine/simplemine.cgi). All pairwise protein alignments were performed using the Pairwise Aligner tool from Biopython[93] with a gap score of -12, an open gap score of -0.5 and a maximum of 10,000 possible alignments.

Meiotic Failure Scoring

Immunofluorescence images of early embryos were scored for meiotic failure by counting polar bodies visible outside of the embryo. Meiotic failures were categorized as follows, no polar body visible, one polar body visible, or both polar bodies visible. DNA capture was scored as positive if chromosomes were in contact with microtubule asters outside of the central spindle.

P-cell division phenotype

P-cell division timing was scored as before AB cell division, same time as AB cell division, and after AB cell division.

Quantification and Statistical Analysis

All graphs shown in the manuscript were created and analyzed in R (Rstudio).[92] Statistical details of experiments can be found in the figure legends.

Video S1. Similar phenotypes are observed after RNAi of *par-2* and *par-6* in *C. elegans* and *C. brenneri* (related to Figures 1D and **S1D).** Timelapse sequences of *C. brenneri* (*top row*) and *C. elegans* embryos (*bottom row*). Control embryos are shown on the left, *par-2(RNAi)* embryos in the middle and *par-6(RNAi)* embryos on the right. Still images of the *C. brenneri par-6(RNAi)* and *par-2(RNAi)* embryos shown here are also shown in *Figure 1D*. Cleavage sites in the *par-2(RNAi)* (*yellow arrows*) and *par-6(RNAi)* (*orange arrows*) embryos are indicated. 26 x 1μm z-stacks were collected every 30 seconds and movies were created by compiling the best z-slice from the z-stack collected at each timepoint. Playback frame rate is 5 frames/second.

Video S2. The sperm pronucleus remains small leading to centrosome detachment in hybrids of *C. brenneri* females and *C. elegans* males (related to Figures 2C-E, S2B, and **S2C)** (00:00 – 00:21 seconds). Representative timelapse sequences showing centriole position and nuclear size during the first cell division in a *C. elegans* embryo

(*top row*) and a *C. brenneri* x *C. elegans* hybrid (*bottom row*). Still images of the wild-type and hybrid embryos shown are also included in *Figures 2D* and *S2B*. Yellow arrows point to the centrosomes. Black dotted lines trace the outline of the pronuclei. Movies are composed of a single z DIC slice overlaid with fluorescence maximum intensity projections of 19 x 1.5 μm z-stacks acquired every 30 seconds. Intensity values for centrioles were scaled to best highlight centrosome positioning are not comparable between different embryos. Playback rate is 5 frames/s.

Aberrant spindle morphologies are observed in hybrid embryos of *C. brenneri* females and *C. elegans* males (related to Figures 3D and **S2E)** (00:22 – 00:32 seconds)**.** Representative timelapse sequences showing centrioles (*green*) and microtubules (*red*) in reference *C. brenneri* (first column) and *C. elegans* (second column) embryos along with two *C. brenneri* x *C. elegans* hybrids. Sequences run from ooctye pronuclear appearance through the first cell division. Still images of the embryos shown are also included in *Figure 3D*. The centrioles (*yellow arrows*), aberrant spindle morphology (*cyan arrows*), and meiotic spindle capture (*dark blue arrows*) are indicated. A 27 x 1 μm z-stack was collected every minute, and movies are composed of maximum intensity projections of the subset of z-planes that best show centrosomes and spindles for each timepoint. Intensity values for spindles are not comparable between different embryos because of the variable amount of dye that may enter the embryo. Playback speed is 5 frames/second.

Video S3. A similar suite of early defects is observed in hybrids between *C. brenneri* females and males from three Elegans group species (related to Figures 4B-D, 1D, 1E, S1A and **S3B)** (00:00 – 00:30 seconds)**.** Representative timelapse sequences of the early embryonic cell divisions in wild-type *C. brenneri*, *C. sp. 48*, *C. remanei* and *C. elegans* embryos (top row) along with their hybrids (*bottom row*). Still images of embryos shown are also included in *Figures 4B*, *S1A* (*Disorganized/other)* and *S3*. Black dotted lines trace pronuclei. Movies are composed of single z-slices chosen from 26 x 1 μm z-stacks acquired every 30sec. Playback rate is 5 frames/second. ***C. sinica* hybrids are characterized by polarity and cell division timing defects (related to Figures 4D-F, S3C,** and **S3D)** (00:31 – 00:55 seconds)**.** Representative timelapse sequences of the early embryonic cell divisions in wild-type *C. sinica* and *C. remanei* (top row) along with their hybrid (bottom row). Stil images of wild-type embryos shown are also included in *Figure 4F*. Black dotted lines trace pronuclei. Movies are composed of single z-slices chosen from 26 x 1 μm z-stacks acquired every 30sec. Playback rate is 5 frames/second.

Data S1. Description of manual scoring data and measured features (related to Figures 3, 4, S3 and STAR Methods). In *Data S1A*, each cross type is highlighted in a different color. NS means the embryo was not scored due to the event not being in view or occurring prior to when the movie initiated. In *Data S1B*, rows highlighted in yellow consistently showed a phenotype during embryo scoring and thus were the scoring parameters used for heat map in *Figures 4C* and *S3D*.

REFERENCES:

1. Coyne, J. A. & Orr, H. A. (1989). Patterns of reproductive isolation in Drosophila. *Evolution* **43**, 362–381.
2. Dobzhansky, T. (1937). *Genetics and the Origin of Species, By Theodosius Dobzhansky*.
3. Mayr, E. (1963). *Animal Species and Evolution*. (Harvard University Press).
4. Mayr, E. (1970). *Populations, Species, and Evolution: An Abridgment of Animal Species and Evolution*. vol. 19 (Harvard University Press).
5. Kitano, J. & Okude, G. (2024). Causative genes of intrinsic hybrid incompatibility in animals and plants: what we have learned about speciation from the molecular perspective. *Evolutionary Journal of the Linnean Society* **3**, kzae022.
6. Mack, K. L. & Nachman, M. W. (2017). Gene Regulation and Speciation. *Trends in Genetics* **33**, 68–80.
7. Wittkopp, P. J., Haerum, B. K. & Clark, A. G. (2004). Evolutionary changes in cis and trans gene regulation. *Nature* **430**, 85–88.
8. Coolon, J. D., McManus, C. J., Stevenson, K. R., Graveley, B. R. & Wittkopp, P. J. (2014). Tempo and mode of regulatory evolution in Drosophila. *Genome Research* **24**, 797–808.
9. Landry, C. R., Wittkopp, P. J., Taubes, C. H., Ranz, J. M., Clark, A. G. & Hartl, D. L. (2005). Compensatory cis-trans Evolution and the Dysregulation of Gene Expression in Interspecific Hybrids of Drosophila. **1822**, 1813–1822.
10. Orr, H. A. & Presgraves, D. C. (2000). Speciation by postzygotic isolation: forces, genes and molecules. *Bioessays* **22**, 1085–1094.
11. Ortíz-Barrientos, D., Counterman, B. A. & Noor, M. A. F. (2006). Gene expression divergence and the origin of hybrid dysfunctions. *Genetica* **129**, 71–81.
12. Shropshire, J. D., Leigh, B. & Bordenstein, S. R. (2020). Symbiont-mediated cytoplasmic incompatibility: What have we learned in 50 years? *eLife* **9**, e61989.

13. Tang, S. & Presgraves, D. C. (2009). Evolution of the *Drosophila* Nuclear Pore Complex Results in Multiple Hybrid Incompatibilities. *Science* **323**, 779–782.
14. Ferree, P. M. & Barbash, D. A. (2009). Species-Specific Heterochromatin Prevents Mitotic Chromosome Segregation to Cause Hybrid Lethality in Drosophila. *PLoS Biol* **7**, e1000234.
15. Ferree, P. M. & Prasad, S. (2012). How Can Satellite DNA Divergence Cause Reproductive Isolation? Let Us Count the Chromosomal Ways. *Genetics Research International* **2012**, 1–11.
16. Presgraves, D. C. (2010). The molecular evolutionary basis of species formation. *Nat Rev Genet* **11**, 175–180.
17. Brand, C. L. & Levine, M. T. (2022). Cross-species incompatibility between a DNA satellite and the Drosophila Spartan homolog poisons germline genome integrity. *Current Biology* **32**, 2962-2971.e4.
18. Kitaoka, M., Smith, O. K., Straight, A. F. & Heald, R. (2022). Molecular conflicts disrupting centromere maintenance contribute to Xenopus hybrid inviability. *Current Biology* **32**, 3939-3951.e6.
19. Brand, C. L. & Levine, M. T. (2021). Functional Diversification of Chromatin on Rapid Evolutionary Timescales. *Annu. Rev. Genet.* **55**, 401–425.
20. Bundus, J. D., Alaei, R. & Cutter, A. D. (2015). Gametic selection, developmental trajectories, and extrinsic heterogeneity in Haldane's rule. *Evolution* **69**, 2005–2017.
21. Bundus, J. D., Wang, D. & Cutter, A. D. (2018). Genetic basis to hybrid inviability is more complex than hybrid male sterility in Caenorhabditis nematodes. *Heredity* **121**, 169–182.
22. Dey, A., Jin, Q., Chen, Y. C. & Cutter, A. D. (2014). Gonad morphogenesis defects drive hybrid male sterility in asymmetric hybrid breakdown of Caenorhabditis nematodes. *Evolution and Development* **16**, 362–372.
23. Kozlowska, J. L., Ahmad, A. R., Jahesh, E. & Cutter, A. D. (2011). GENETIC VARIATION FOR POSTZYGOTIC REPRODUCTIVE ISOLATION BETWEEN CAENORHABDITIS BRIGGSAE AND. 1180–1195 doi:10.1111/j.1558-5646.2011.01514.x.

24. Woodruff, G. C., Eke, O., Baird, S. E., Félix, M. A. & Haag, E. S. (2010). Insights into species divergence and the evolution of hermaphroditism from fertile interspecies hybrids of Caenorhabditis nematodes. *Genetics* **186**, 997–1012.

25. Baird, S. E. & Seibert, S. R. (2013). Reproductive isolation in the Elegans-Group of Caenorhabditis. **5**, 18–25.

26. Rockman, M. V., Ailion, M., Braendle, C., Fitch, D. H., Pénigault, J.-B., Félix, M.-A. & Kiontke, K. C. (2011). A phylogeny and molecular barcodes for Caenorhabditis, with numerous new species from rotting fruits. *BMC Evolutionary Biology* **11**, 339.

27. Baird, S. E. & Yen, W. C. (2000). Reproductive isolation in Caenorhabditis: Terminal phenotypes of hybrid embryos. *Evolution and Development* doi:10.1046/j.1525-142X.2000.00031.x.

28. Baird, S. E., Sutherlin, M. E. & Emmons, S. W. (1992). REPRODUCTIVE ISOLATION IN RHABDITIDAE (NEMATODA: SECERNENTEA); MECHANISMS THAT ISOLATE SIX SPECIES OF THREE GENERA. *Evolution* **46**, 585–594.

29. Baugh, L. R., Hill, A. A., Slonim, D. K., Brown, E. L. & Hunter, C. P. (2003). Composition and dynamics of the *Caenorhabditis elegans* early embryonic transcriptome. *Development* **130**, 889–900.

30. Guven-Ozkan, T., Nishi, Y., Robertson, S. M. & Lin, R. (2008). Global Transcriptional Repression in C. elegans Germline Precursors by Regulated Sequestration of TAF-4. *Cell* **135**, 149–160.

31. Stoeckius, M., Grün, D. & Rajewsky, N. (2014). Paternal RNA contributions in the Caenorhabditis elegans zygote. *The EMBO Journal* **33**, 1740–1750.

32. Macchietto, M., Angdembey, D., Heidarpour, N., Serra, L., Rodriguez, B., El-Ali, N. & Mortazavi, A. (2017). Comparative Transcriptomics of Steinernema and Caenorhabditis Single Embryos Reveals Orthologous Gene Expression Convergence during Late Embryogenesis. *Genome Biology and Evolution* **9**, 2681–2696.

33. Boveri, T. (1888). Zellenstudien II: Die Befruchtung und Teilung des Eies von Ascaris megalocephala. *Jenaer Zeitschrift für Naturwissenschaft* 685–882, plates XIX-XXIII.

34. Albertson, D. G. (1984). Formation of the first cleavage spindle in nematode embryos. *Developmental Biology* **101**, 61–72.
35. Wolf, N., Hirsh, D. & McIntosh, J. R. (1978). Spermatogenesis in males of the free-living nematode, Caenorhabditis elegans. *Journal of Ultrastructure Research* **63**, 155–169.
36. Smith, J. R. & Stanfield, G. M. (2012). A seminal fluid protease activates sperm motility in C. elegans males. *Worm* **1**, 151–154.
37. L'Hernault, S. W. (2006). Spermatogenesis. *WormBook: the online review of C. elegans biology [Internet]*.
38. Chu, D. S. & Shakes, D. C. (2012). Spermatogenesis. *Germ cell development in C. elegans* 171–203.
39. Oegema, K. (2006). Cell division. *WormBook* doi:10.1895/wormbook.1.72.1.
40. McNally, K. L. P., Fabritius, A. S., Ellefson, M. L., Flynn, J. R., Milan, J. A. & McNally, F. J. (2012). Kinesin-1 Prevents Capture of the Oocyte Meiotic Spindle by the Sperm Aster. *Developmental Cell* **22**, 788–798.
41. Severson, A. F., Von Dassow, G. & Bowerman, B. (2016). Oocyte Meiotic Spindle Assembly and Function. in *Current Topics in Developmental Biology* vol. 116 65–98 (Elsevier).
42. Cowan, C. R. & Hyman, A. A. (2004). Centrosomes direct cell polarity independently of microtubule assembly in C. elegans embryos. *Nature* **431**, 92–96.
43. Rose, L. & Gonczy, P. (2014). Polarity establishment, asymmetric division and segregation of fate determinants in early C. elegans embryos. *WormBook* 1–43 doi:10.1895/wormbook.1.30.2.
44. Dey, A., Chan, C. K. W., Thomas, C. G. & Cutter, A. D. (2013). Molecular hyperdiversity defines populations of the nematode Caenorhabditis brenneri. doi:10.1073/pnas.1303057110/-/DCSupplemental.www.pnas.org/cgi/doi/10.1073/pnas.1303057110.
45. Barriere, A., Yang, S.-P., Pekarek, E., Thomas, C. G., Haag, E. S. & Ruvinsky, I. Detecting heterozygosity in shotgun genome assemblies: Lessons from obligately outcrossing nematodes.

46. Wang, S. *et al.* (2019). A high-content imaging approach to profile *C. elegans* embryonic development. *Development* dev.174029 doi:10.1242/dev.174029.

47. Green, R. A. *et al.* (2024). Automated profiling of gene function during embryonic development. *Cell* **187**, 3141-3160.e23.

48. Sönnichsen, B. *et al.* (2005). Full-genome RNAi profiling of early embryogenesis in Caenorhabditis elegans. *Nature* **434**, 462–469.

49. Cuenca, A. A., Schetter, A., Aceto, D., Kemphues, K. & Seydoux, G. (2003). Polarization of the C. elegans zygote proceeds via distinct establishment and maintenance phases. *Development* **130**, 1255–1265.

50. Munro, E., Nance, J. & Priess, J. R. (2004). Cortical Flows Powered by Asymmetrical Contraction Transport PAR Proteins to Establish and Maintain Anterior-Posterior Polarity in the Early C. elegans Embryo. *Developmental Cell* **7**, 413–424.

51. Bienkowska, D. & Cowan, C. R. (2012). Centrosomes Can Initiate a Polarity Axis from Any Position within One-Cell C. elegans Embryos. *Current Biology* **22**, 583–589.

52. Hoege, C. & Hyman, A. A. (2013). Principles of PAR polarity in Caenorhabditis elegans embryos. *Nat Rev Mol Cell Biol* **14**, 315–322.

53. Boyd, L., Guo, S., Levitan, D., Stinchcomb, D. T. & Kemphues, K. J. (1996). PAR-2 is asymmetrically distributed and promotes association of P granules and PAR-1 with the cortex in *C. elegans* embryos. *Development* **122**, 3075–3084.

54. Hoege, C., Constantinescu, A.-T., Schwager, A., Goehring, N. W., Kumar, P. & Hyman, A. A. (2010). LGL Can Partition the Cortex of One-Cell Caenorhabditis elegans Embryos into Two Domains. *Current Biology* **20**, 1296–1303.

55. Hannak, E., Kirkham, M., Hyman, A. A. & Oegema, K. (2001). Aurora-A kinase is required for centrosome maturation in *Caenorhabditis elegans*. *The Journal of Cell Biology* **155**, 1109–1116.

56. Hamill, D. R., Severson, A. F., Carter, J. C. & Bowerman, B. (2002). Centrosome Maturation and Mitotic Spindle Assembly in C. elegans Require SPD-5, a Protein with Multiple Coiled-Coil Domains. *Developmental Cell* **3**, 673–684.

57. Hannak, E., Oegema, K., Kirkham, M., Gönczy, P., Habermann, B. & Hyman, A. A. (2002). The kinetically dominant assembly pathway for centrosomal asters in *Caenorhabditis elegans* is γ-tubulin dependent. *The Journal of Cell Biology* **157**, 591–602.

58. Ohta, M., Zhao, Z., Wu, D., Wang, S., Harrison, J. L., Gómez-Cavazos, J. S., Desai, A. & Oegema, K. F. (2021). Polo-like kinase 1 independently controls microtubule-nucleating capacity and size of the centrosome. *Journal of Cell Biology* **220**, e202009083.

59. Malone, C. J., Misner, L., Le Bot, N., Tsai, M.-C., Campbell, J. M., Ahringer, J. & White, J. G. (2003). The C. elegans Hook Protein, ZYG-12, Mediates the Essential Attachment between the Centrosome and Nucleus. *Cell* **115**, 825–836.

60. Minn, I., Rolls, M. M., Hanna-Rose, W. & Malone, C. J. (2009). SUN-1 and ZYG-12, Mediators of Centrosome–Nucleus Attachment, Are a Functional SUN/KASH Pair in Caenorhabditis elegans. *MBoC* **20**, 4586–4595.

61. Gönczy, P., Pichler, S., Kirkham, M. & Hyman, A. A. (1999). Cytoplasmic Dynein Is Required for Distinct Aspects of Mtoc Positioning, Including Centrosome Separation, in the One Cell Stage *Caenorhabditis elegans* Embryo. *The Journal of Cell Biology* **147**, 135–150.

62. Meyerzon, M., Gao, Z., Liu, J., Wu, J.-C., Malone, C. J. & Starr, D. A. (2009). Centrosome attachment to the C. elegans male pronucleus is dependent on the surface area of the nuclear envelope. *Developmental Biology* **327**, 433–446.

63. Grill, S. W., Gönczy, P., Stelzer, E. H. K. & Hyman, A. A. (2001). Polarity controls forces governing asymmetric spindle positioning in the Caenorhabditis elegans embryo. *Nature* **409**, 630–633.

64. Cheng, N. N., Kirby, C. M. & Kemphues, K. J. (1995). Control of Cleavage Spindle Orientation in Caenorhabditis elegans: The Role of the Genes par-2 and par-3. doi:10.1093/genetics/139.2.549.

65. McNally, K. L. & McNally, F. J. (2005). Fertilization initiates the transition from anaphase I to metaphase II during female meiosis in C. elegans. *Developmental Biology* **282**, 218–230.
66. Picao-Osorio, J., Bouleau, C., Gonzalez De La Rosa, P. M., Stevens, L., Fekonja, N., Blaxter, M., Braendle, C. & Félix, M.-A. (2025). Evolution of developmental bias explains divergent patterns of phenotypic evolution. Preprint at https://doi.org/10.1101/2025.02.04.636455.
67. Cutter, A. D. (2008). Divergence Times in Caenorhabditis and Drosophila Inferred from Direct Estimates of the Neutral Mutation Rate. *Molecular Biology and Evolution* **25**, 778–786.
68. Stevens, L. (2020). Genome evolution in the genus Caenorhabditis. *University of Edinburgh* **Ph.D. Dissertation**,.
69. Ward, S., Argon, Y. & Nelson, G. A. (1981). Sperm morphogenesis in wild-type and fertilization-defective mutants of Caenorhabditis elegans. *The Journal of cell biology* **91**, 26–44.
70. Li, D., Huang, S., Chai, Y., Zhao, R., Gong, J., Zhang, Q. C., Ou, G. & Wen, W. (2023). A paternal protein facilitates sperm RNA delivery to regulate zygotic development. *Sci. China Life Sci.* **66**, 2342–2353.
71. Hill, D. P., Shakes, C., Ward, S. & Strome, S. (1989). A Sperm-Supplied Product Essential for Initiation of Normal Embryogenesis in Caenorhabditis elegans Is Encoded by the Paternal-Effect Embryonic-Lethal Gene, spe-7 I. doi:10.1016/0012-1606(89)90138-3.
72. Kasimatis, K. R. & Phillips, P. C. (2018). Rapid Gene Family Evolution of a Nematode Sperm Protein Despite Sequence Hyper-conservation. *G3 Genes|Genomes|Genetics* **8**, 353–362.
73. Galy, V., Askjaer, P., Franz, C., López-Iglesias, C. & Mattaj, I. W. (2006). MEL-28, a Novel Nuclear-Envelope and Kinetochore Protein Essential for Zygotic Nuclear-Envelope Assembly in C. elegans. *Current Biology* **16**, 1748–1756.
74. Gómez-Saldivar, G. *et al.* (2016). Identification of Conserved MEL-28/ELYS Domains with Essential Roles in Nuclear Assembly and Chromosome Segregation. *PLOS Genetics*.
75. Askjaer, P. Modern Tools to Study Nuclear Pore Complexes and Nucleocytoplasmic Transport in Caenorhabditis elegans.

826 76. Martino, L., Joly, N. & Desai, A. Channel Nucleoporins Recruit PLK-1 to Nuclear Pore Complexes
827 to Direct Nuclear Envelope Breakdown in C. elegans.
828 77. Voronina, E. & Seydoux, G. The C. elegans homolog of nucleoporin Nup98 is required for the
829 integrity and function of germline P granules.
830 78. Walther, T. C., Fornerod, M., Pickersgill, H., Goldberg, M., Allen, T. D. & Mattaj, I. W. (2001). The
831 nucleoporin Nup153 is required for nuclear pore basket formation, nuclear pore complex anchoring
832 and import of a subset of nuclear proteins. *The EMBO journal*.
833 79. Ródenas, E., González-Aguilera, C., Ayuso, C. & Askjaer, P. (2012). Dissection of the NUP107
834 nuclear pore subcomplex reveals a novel interaction with spindle assembly checkpoint protein
835 MAD1 in *Caenorhabditis elegans*. *MBoC* **23**, 930–944.
836 80. Waddington, C. H. (1942). Canalization of development and the inheritance of acquired characters.
837 *Nature* **150**, 563–565.
838 81. Dammermann, A., Müller-Reichert, T., Pelletier, L., Habermann, B., Desai, A. & Oegema, K. (2004).
839 Centriole Assembly Requires Both Centriolar and Pericentriolar Material Proteins. *Developmental*
840 *Cell* **7**, 815–829.
841 82. Stiernagle, T. (2006). Maintenance of C.elegans. in *WormBook* 1–11
842 doi:10.1895/wormbook.1.101.1.
843 83. Van Rossum, G. & Drake Jr, F. L. (1995). *Python Tutorial*. vol. 620 (Centrum voor Wiskunde en
844 Informatica Amsterdam, The Netherlands).
845 84. Anderson, J. L., Morran, L. T. & Phillips, P. C. (2010). Outcrossing and the Maintenance of Males
846 within C. elegans Populations. *Journal of Heredity* **101**, S62–S74.
847 85. Ebert, M. S. Evolution remodels olfactory and mating-receptive behaviors in the transition from
848 female to hermaphrodite reproduction. *OPEN ACCESS*.
849 86. Bao, Z. & Murray, J. I. (2011). Mounting *Caenorhabditis elegans* Embryos for Live Imaging of
850 Embryogenesis: Figure 1. *Cold Spring Harb Protoc* **2011**, pdb.prot065599.

87. Tagawa, A., Rappleye, C. A. & Aroian, R. V. (2001). pod-2, along with pod-1, Defines a New Class of Genes Required for Polarity in the Early Caenorhabditis elegans Embryo. *Developmental Biology* **233**, 412–424.

88. Edgar, L. G. (1995). Chapter 13 Blastomere Culture and Analysis. in *Methods in Cell Biology* vol. 48 303–321 (Elsevier).

89. Schindelin, J. *et al.* (2012). Fiji: an open-source platform for biological-image analysis. *Nat Methods* **9**, 676–682.

90. Oegema, K., Desai, A., Rybina, S., Kirkham, M. & Hyman, A. A. (2001). Functional Analysis of Kinetochore Assembly in *Caenorhabditis elegans*. *The Journal of Cell Biology* **153**, 1209–1226.

91. Emms, D. M. & Kelly, S. (2019). OrthoFinder: phylogenetic orthology inference for comparative genomics. *Genome Biol* **20**, 238.

92. R Core Team. (2023). R: A Language and Environment for Statistical Computing. R Foundation for Statistical Computing.

93. Cock, P. J. *et al.* (2009). Biopython: freely available Python tools for computational molecular biology and bioinformatics. *Bioinformatics* **25**, 1422.

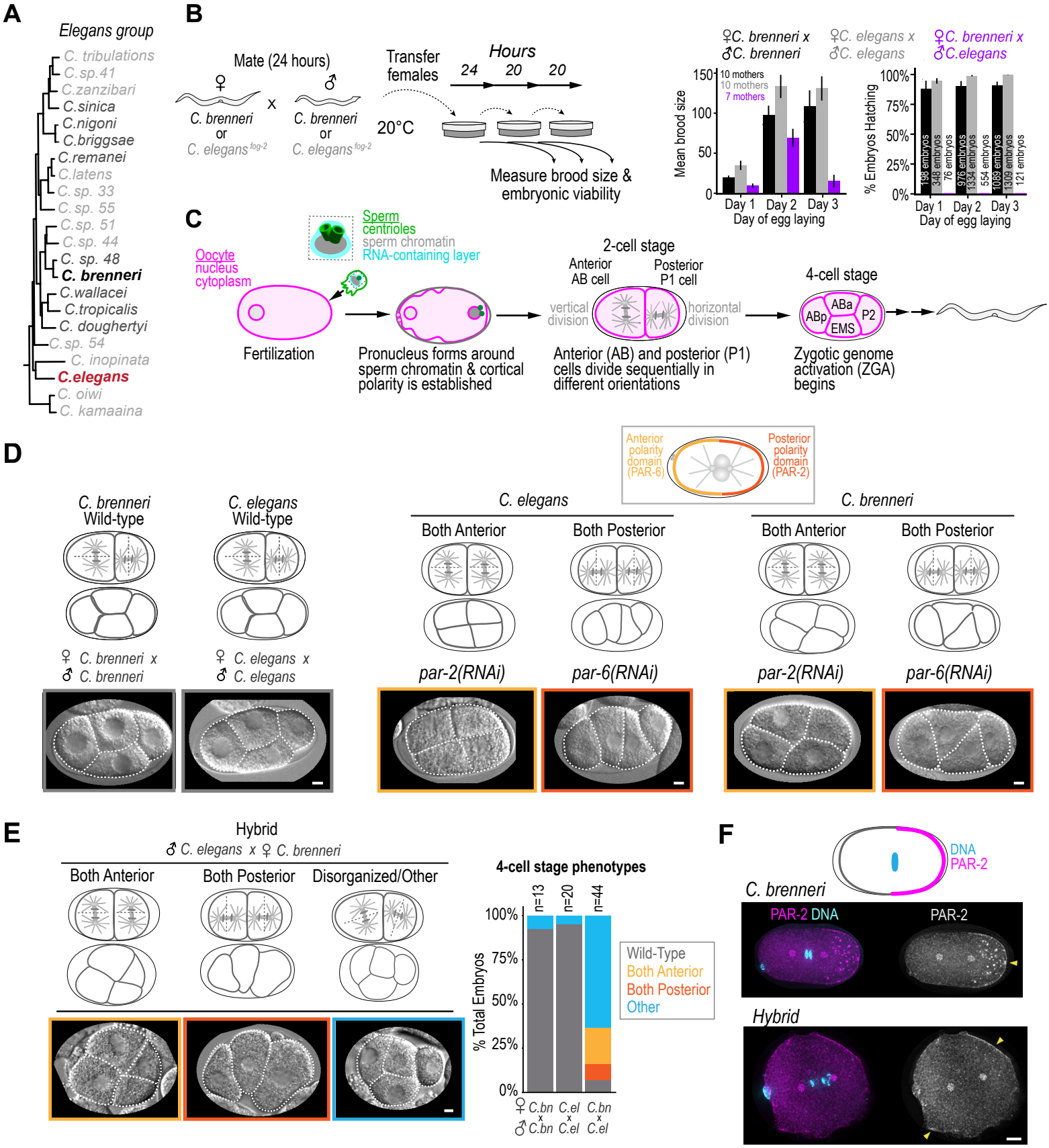
A
Elegans group
C. tribulations
C. sp.41
C.zanzibari
C.sinica
C.nigoni
C.briggsae
C.remanei
C.latens
C. sp. 33
C. sp. 55
C.sp. 51
C.sp. 44
C. sp. 48
C. brenneri
C.wallacei
C.tropicalis
C. doughertyi
C.sp. 54
C. inopinata
C.elegans
C. oiwi
C. kamaaina
B
Mate (24 hours)
C. brenneri or C. elegans fog-2
x
C. brenneri or C. elegans fog-2
Transfer females
Hours
24
20
20
20°C
Measure brood size & embryonic viability
♀C. brenneri x ♂C. brenneri
♀C. elegans x ♂C. elegans
♀C. brenneri x ♂C.elegans
Mean brood size
10 mothers
10 mothers
7 mothers
Day 1
Day 2
Day 3
Day of egg laying
% Embryos Hatching
198 embryos
348 embryos
76 embryos
976 embryos
1334 embryos
554 embryos
1089 embryos
1309 embryos
121 embryos
C
Sperm centrioles
sperm chromatin
RNA-containing layer
Oocyte nucleus
cytoplasm
Fertilization
Pronucleus forms around sperm chromatin & cortical polarity is established
2-cell stage
Anterior AB cell
Posterior P1 cell
vertical division
horizontal division
Anterior (AB) and posterior (P1) cells divide sequentially in different orientations
4-cell stage
ABa
ABp
EMS
P2
Zygotic genome activation (ZGA) begins
D
Anterior polarity domain (PAR-6)
Posterior polarity domain (PAR-2)
C. brenneri Wild-type
C. elegans Wild-type
♀ C. brenneri x ♂ C. brenneri
♀ C. elegans x ♂ C. elegans
C. elegans
C. brenneri
Both Anterior
Both Posterior
par-2(RNAi)
par-6(RNAi)
E
Hybrid
♂ C. elegans x ♀ C. brenneri
Both Anterior
Both Posterior
Disorganized/Other
4-cell stage phenotypes
% Total Embryos
n=13
n=20
n=44
Wild-Type
Both Anterior
Both Posterior
Other
♀C.bn x ♂C.bn
C.el x C.el
C.bn x C.el
F
DNA
PAR-2
C. brenneri
PAR-2 DNA
PAR-2
Hybrid

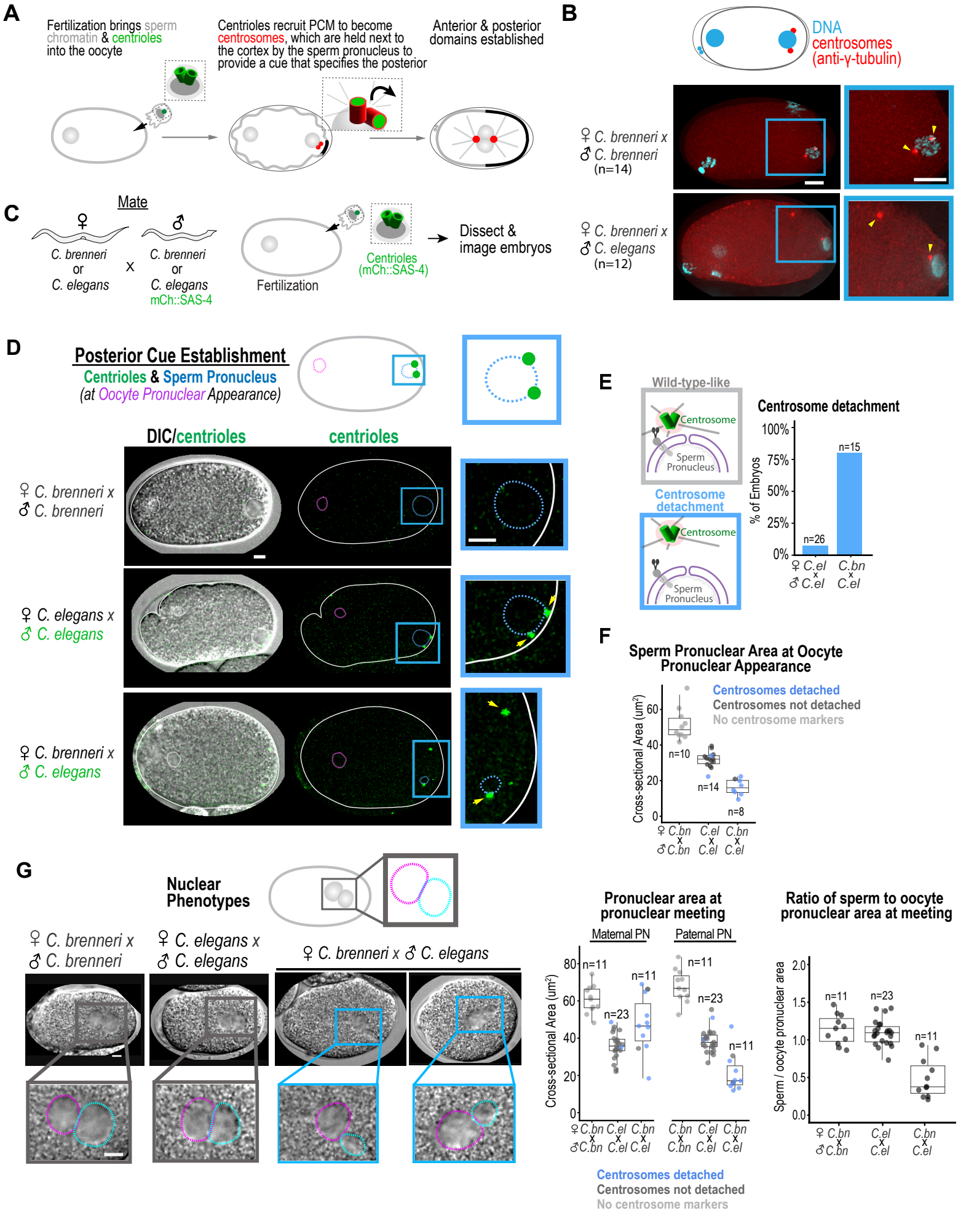
A
Fertilization brings sperm chromatin & centrioles into the oocyte
Centrioles recruit PCM to become centrosomes, which are held next to the cortex by the sperm pronucleus to provide a cue that specifies the posterior
Anterior & posterior domains established
B
DNA
centrosomes (anti-γ-tubulin)
♀ C. brenneri x ♂ C. brenneri (n=14)
♀ C. brenneri x ♂ C. elegans (n=12)
C
Mate
C. brenneri or C. elegans
x
C. brenneri or C. elegans mCh::SAS-4
Fertilization
Centrioles (mCh::SAS-4)
Dissect & image embryos
D
Posterior Cue Establishment
Centrioles & Sperm Pronucleus
(at Oocyte Pronuclear Appearance)
DIC/centrioles
centrioles
♀ C. brenneri x ♂ C. brenneri
♀ C. elegans x ♂ C. elegans
♀ C. brenneri x ♂ C. elegans
E
Wild-type-like
Centrosome
Sperm Pronucleus
Centrosome detachment
Centrosome detachment
% of Embryos
100%
75%
50%
25%
0%
n=26
n=15
♀ C.el x ♂ C.el
C.bn x C.el
F
Sperm Pronuclear Area at Oocyte Pronuclear Appearance
Centrosomes detached
Centrosomes not detached
No centrosome markers
Cross-sectional Area (um²)
n=10
n=14
n=8
♀ C.bn x ♂ C.bn
C.el x C.el
C.bn x C.el
G
Nuclear Phenotypes
♀ C. brenneri x ♂ C. brenneri
♀ C. elegans x ♂ C. elegans
♀ C. brenneri x ♂ C. elegans
Pronuclear area at pronuclear meeting
Maternal PN
Paternal PN
Cross-sectional Area (um²)
n=11
n=23
n=11
n=11
n=23
n=11
Ratio of sperm to oocyte pronuclear area at meeting
Sperm / oocyte pronuclear area
n=11
n=23
n=11
Centrosomes detached
Centrosomes not detached
No centrosome markers

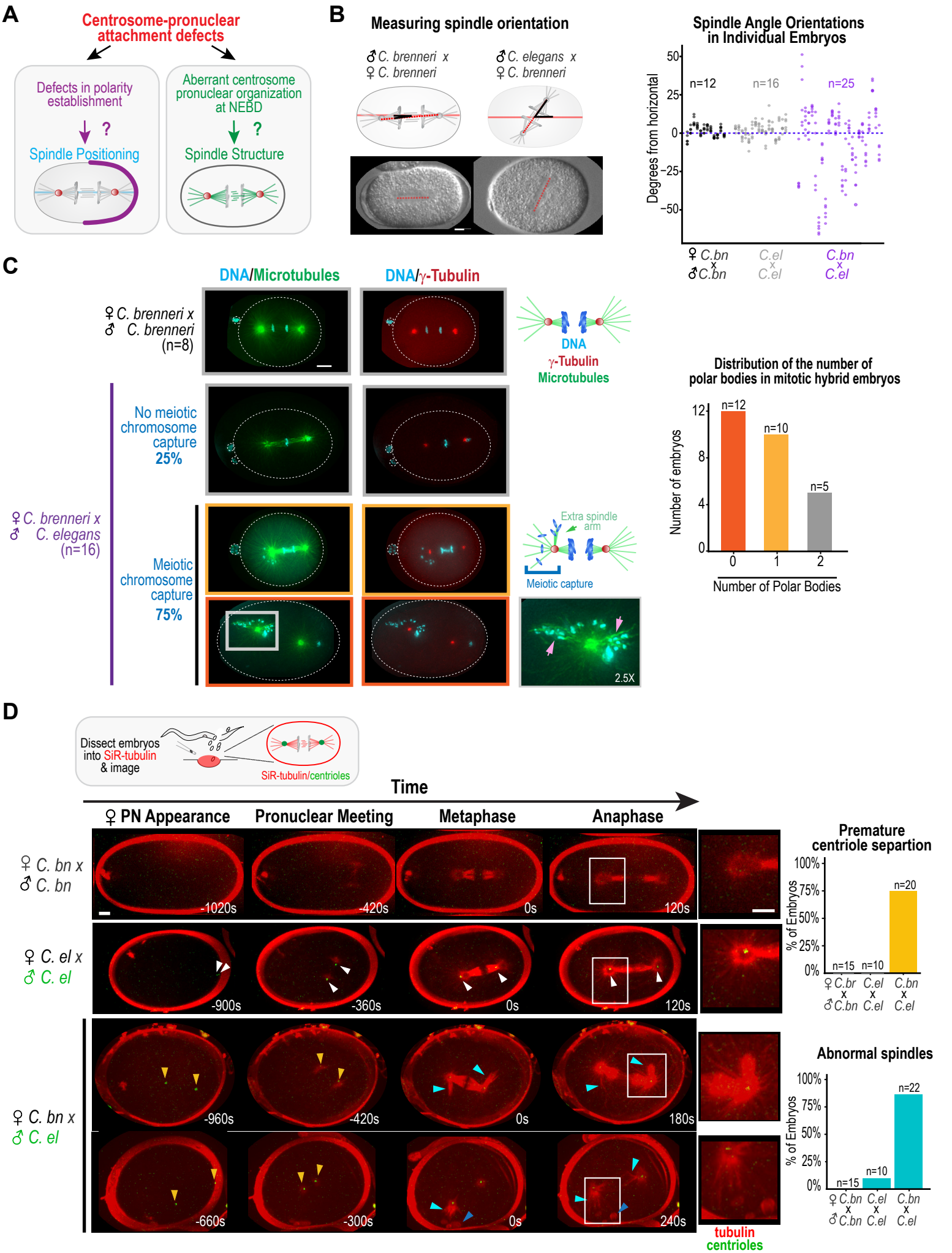
A
Centrosome-pronuclear attachment defects
Defects in polarity establishment
?
Spindle Positioning
Aberrant centrosome pronuclear organization at NEBD
?
Spindle Structure
B
Measuring spindle orientation
♂C. brenneri x ♀C. brenneri
♂C. elegans x ♀C. brenneri
Spindle Angle Orientations in Individual Embryos
Degrees from horizontal
50
25
0
−25
−50
n=12
n=16
n=25
♀C.bn x ♂C.bn
C.el x C.el
C.bn x C.el
C
DNA/Microtubules
DNA/γ-Tubulin
♀C. brenneri x ♂ C. brenneri (n=8)
DNA
γ-Tubulin
Microtubules
No meiotic chromosome capture 25%
♀C. brenneri x ♂ C. elegans (n=16)
Meiotic chromosome capture 75%
Extra spindle arm
Meiotic capture
2.5X
Distribution of the number of polar bodies in mitotic hybrid embryos
Number of embryos
12
8
4
0
n=12
n=10
n=5
0
1
2
Number of Polar Bodies
D
Dissect embryos into SiR-tubulin & image
SiR-tubulin/centrioles
Time
♀ PN Appearance
Pronuclear Meeting
Metaphase
Anaphase
♀ C. bn x ♂ C. bn
-1020s
-420s
0s
120s
♀ C. el x ♂ C. el
-900s
-360s
0s
120s
♀ C. bn x ♂ C. el
-960s
-420s
0s
180s
-660s
-300s
0s
240s
tubulin
centrioles
Premature centriole separtion
% of Embryos
100%
75%
50%
25%
0%
n=15
n=10
n=20
♀C.br x ♂C.bn
C.el x C.el
C.bn x C.el
Abnormal spindles
% of Embryos
100%
75%
50%
25%
0%
n=15
n=10
n=22
♀C.bn x ♂C.bn
C.el x C.el
C.bn x C.el

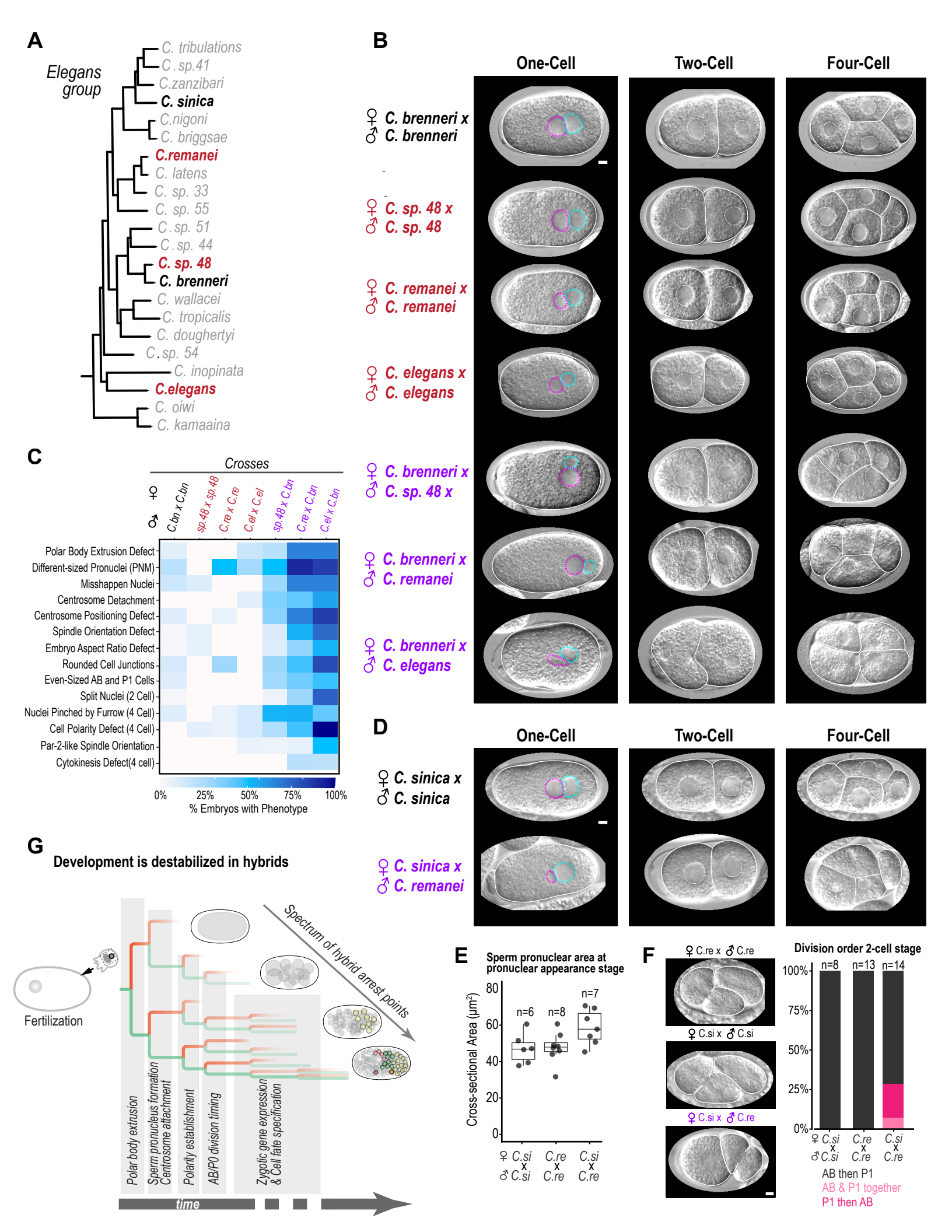
A
Elegans group
C. tribulations
C . sp.41
C.zanzibari
C. sinica
C.nigoni
C. briggsae
C.remanei
C. latens
C. sp. 33
C. sp. 55
C . sp. 51
C . sp. 44
C. sp. 48
C. brenneri
C. wallacei
C. tropicalis
C. doughertyi
C . sp. 54
C. inopinata
C.elegans
C. oiwi
C. kamaaina
B
One-Cell
Two-Cell
Four-Cell
♀ C. brenneri x ♂ C. brenneri
♀ C. sp. 48 x ♂ C. sp. 48
♀ C. remanei x ♂ C. remanei
♀ C. elegans x ♂ C. elegans
♀ C. brenneri x ♂ C. sp. 48 x
♀ C. brenneri x ♂ C. remanei
♀ C. brenneri x ♂ C. elegans
C
Crosses
♀
♂
C.bn x C.bn
sp.48 x sp.48
C.re x C.re
C.el x C.el
sp.48 x C.bn
C.re x C.bn
C.el x C.bn
Polar Body Extrusion Defect
Different-sized Pronuclei (PNM)
Misshappen Nuclei
Centrosome Detachment
Centrosome Positioning Defect
Spindle Orientation Defect
Embryo Aspect Ratio Defect
Rounded Cell Junctions
Even-Sized AB and P1 Cells
Split Nuclei (2 Cell)
Nuclei Pinched by Furrow (4 Cell)
Cell Polarity Defect (4 Cell)
Par-2-like Spindle Orientation
Cytokinesis Defect(4 cell)
0%
25%
50%
75%
100%
% Embryos with Phenotype
D
One-Cell
Two-Cell
Four-Cell
♀ C. sinica x ♂ C. sinica
♀ C. sinica x ♂ C. remanei
G
Development is destabilized in hybrids
Fertilization
Spectrum of hybrid arrest points
Polar body extrusion
Sperm pronucleus formation
Centrosome attachment
Polarity establishment
AB/P0 division timing
Zygotic gene expression
& Cell fate specification
time
E
Sperm pronuclear area at pronuclear appearance stage
Cross-sectional Area (µm²)
80
60
40
20
0
n=6
n=8
n=7
♀ C.si x ♂ C.si
C.re x C.re
C.si x C.re
F
♀ C.re x ♂ C.re
♀ C.si x ♂ C.si
♀ C.si x ♂ C.re
Division order 2-cell stage
n=8
n=13
n=14
100%
75%
50%
25%
0%
♀ C.si x ♂ C.si
C.re x C.re
C.si x C.re
AB then P1
AB & P1 together
P1 then AB